



The CDF-II Time-of-Flight Detector

S. Cabrera^a J. Fernández^a G. Gómez^a J. Piedra^a T. Rodrigo^a
A. Ruiz^a I. Vila^{a,1} R. Vilar^a C. Grozis^b R. Kephart^b
R. Stanek^b D. H. Kim^c M. S. Kim^c Y. Oh^c Y. K. Kim^d
G. Veramendi^d K. Anikeev^e G. Bauer^e I. K. Furic^e A. Korn^e
I. Kravchenko^e M. Mulhearn^e C. Paus^e S. Pavlon^e
K. Sumorok^e C. Chen^f M. Jones^f W. Kononenko^f J. Kroll^f
G. M. Mayers^f F. M. Newcomer^f R. G. C. Oldeman^f
D. Usynin^f R. Van Berg^f G. Bellettini^g C. Cerri^g
A. Menzione^g F. Spinella^g E. Vataga^g S. De Cecco^h
D. De Pedis^h C. Dionisi^h S. Giagu^h A. De Girolamo^h
M. Rescigno^h L. Zanello^h M. Ahnⁱ B. J. Kimⁱ S. B. Kimⁱ
I. Cho^j J. Lee^j I. Yu^j H. Kaneko^k A. Kazama^k S. Kim^k
K. Sato^k K. Sato^k F. Ukegawa^k

^a*Instituto de Física de Cantabria, Spain*

^b*Fermi National Accelerator Laboratory, USA*

^c*Kyungpook National University, Korea*

^d*Lawrence Berkeley National Laboratory, USA*

^e*Massachusetts Institute of Technology, USA*

^f*University of Pennsylvania, USA*

^g*INFN, University of Pisa, Italy*

^h*INFN, University of Roma, Italy*

ⁱ*Seoul National University, Korea*

^j*SungKyunKwan University, Korea*

^k*University of Tsukuba, Japan*

Abstract

A Time-of-Flight (TOF) detector, based on plastic scintillator and fine-mesh photomultiplier tubes, has been added to the CDF-II experiment. Since August 2001, the TOF system has been fully instrumented and integrated into the CDF-II data acquisition system. The TOF system will provide particle identification of low momentum charged pions, kaons and protons in $p\bar{p}$ collisions. With a design resolution

goal of about 100 ps, separation between charged kaons and pions is expected at the 2 sigma level for momenta below 1.6 GeV/c, which enhances CDF's b-flavor tagging capabilities. We describe the design of the TOF detector and discuss its on-line and off-line calibration. Some performance benchmarks using proton-antiproton collision data are presented.

Key words: Time-of-Flight; CDF; fine-mesh photomultipliers; Particle identification

1 Introduction

After the successful Run-I data taking period at the Fermilab Tevatron from 1992 to 1996, the CDF detector has undergone a major upgrade [1] for the so called Run-II of the Tevatron, which began in March 2001. A Time-of-Flight (TOF) detector has been added to improve the particle identification capability. The installation of the TOF detector was completed in August 2001 and its data has been included in the CDF-II readout since that time.

During Run-I, particle identification in CDF was based on the ionization energy loss, dE/dx , measured in the central drift chamber. The dE/dx measurement provided one standard deviation separation between charged kaons and charged pions for momenta greater than 2 GeV/c. The CDF-II drift chamber, the Central Outer Tracker (COT), maintains this dE/dx performance. The primary physics motivation for TOF is to enhance the particle identification capability to improve neutral B meson flavor determination at production. With an expected Time-of-Flight resolution of 100 ps, the TOF system will provide at least two standard deviation separation between K^\pm and π^\pm for momenta $p < 1.6$ GeV/c, complementing the dE/dx measurement from the COT.

Particle identification with TOF is performed by measuring the time of arrival of a particle at the scintillator with respect to the collision time, t_0 . The particle mass m can then be determined from the momentum p , the path-length L , and the time-of-Fight t :

$$m = \frac{p}{c} \sqrt{\frac{c^2 t^2}{L^2} - 1} \quad (1)$$

where p and L are measured by the tracking system. Figure 1 shows the separation power between K/π , p/K and p/π for 100 ps time resolution.

¹ Corresponding Author

For comparison, the separation provided by dE/dx is also shown. The TOF system improves substantially the K/π separation in the momentum region $p < 1.6 \text{ GeV}/c$.

2 CDF TOF design

2.1 Mechanics

The CDF Time-of-Flight detector[2–4] consists of 216 bars of Bicron BC-408 scintillator with dimensions $4 \times 4 \times 279 \text{ cm}$ located between the Central Outer Tracker (COT) and the cryostat of the super-conducting solenoid at a mean radius of 140 cm. The pseudo-rapidity coverage of the system is roughly $|\eta| < 1$.

The bars of scintillator were wrapped first in white Tyvek and a layer of black Marvelguard. The bars were assembled in groups of three by interleaving them with thin metal strips attached via springs to the aluminum PMT housing at the ends. The entire assembly was then wrapped again in black Kevlar. The scintillator assemblies at the top of the detector do not have any of their weight supported by the COT, as this could deflect the COT end-plates. Instead, the scintillator assemblies located at ϕ angles between 15° and 165° with respect to the horizontal are held against the surface of the cryostat by a structure made from folded sheet aluminum which was attached using aluminum studs spot welded to the cryostat. The scintillator in the lower part of the detector rests on the bottom of the cryostat and is self-supporting on the sides. This results in deviations from a nominal geometry of equally spaced bars in ϕ , but a photogrammetric survey of the bar positions was carried out after installation to determine their locations. Since then, their surveyed positions have been refined by analyzing collision data and the ϕ angles of the bar centers are currently understood to better than a few mrad.

2.2 Photomultiplier Tubes and assembly

A Hamamatsu R7761 nineteen-stage fine-mesh photomultiplier tube (PMT) with a diameter of 1.5 inches, is attached to each end of every bar. These can operate in the 1.4 Tesla magnetic field of the CDF solenoid with an average gain reduction factor of 500 from the nominal gain of 10^6 . The optical connection between the PMT and the scintillator is made using a compound parabolic concentrator (CPC), attached to the PMT using optical cement. A good interface between the CPC and the scintillator is achieved using a silicone

optical coupling pad that is compressed between them using the force applied by a spring. The voltage divider base is constructed using surface mount components on a printed circuit board, soldered directly to the leads of the PMT. A preamplifier is attached via a connector on the base. A small printed circuit board serves as a light seal and brings high voltage for the base and low voltage for the preamplifier into the assembly and signals from the preamplifier out. This entire assembly is mounted inside a 1.5 inch diameter hole bored in an aluminum block with approximately the same transverse dimensions as the scintillator. A spring forces the assembly against the scintillator, insuring a good connection at the silicone optical coupling pad interface.

2.3 Front End Electronics

Figure 2 shows the signal path for a single PMT channel. The preamplifier receives a nearly differential input formed from the anode and last dynode stage of the PMT. Its differential output is transmitted on shielded twisted pair cable a distance of approximately 12 meters to the front-end electronics that resides in a VME crate mounted outside the detector. The received signal is split between two signal paths: one for the timing measurement and the other for a measurement related to the pulse height.

The timing path enters a discriminator with an adjustable threshold. The discriminator output provides a start signal to a Time-to-Amplitude Converter (TAC). The TAC ramp is terminated by a common stop clock edge. The voltage output from the TAC is sampled by a 12-bit ADC whose data is buffered by a VME module, referred to as the ADMEM[5], which was designed originally to read out PMT signals from CDF's calorimeter systems. The least count of this TDC corresponds to roughly 17 ps and the available dynamic range is typically 60 ns.

The common stop signal has its phase correctly adjusted with respect to the p and \bar{p} bunch crossing time and is fanned out to all electronics channels in the system. This is implemented using a dedicated set of modules that first distributes differential ECL clock signals to each of 8 crates of electronics, and then to six TOF electronics modules within each crate. This same system generates a reset signal for the TAC and distributes it, along with a clock signal used for calibration, to all electronics channels.

The primary purpose for measuring the charge of the PMT signals is to perform a correction for the discriminator walk, or time slewing, due to pulses of varying amplitude. The charge measurement path converts the received voltage signal from the preamplifier into a current that is passed to a charge sensitive ADC located on the ADMEM module. The current driver circuit is

switched by a gate of adjustable width, initiated by the discriminator output, so that only the charge due to the pulse that fired the discriminator is integrated.

In addition to these basic operations, the front-end electronics provides several services necessary for configuration, monitoring, calibration and testing. An FPGA interfaces with one VME register and is used to set all discriminator thresholds and gate widths and to provide control over the state of the calibration and monitoring circuits. Various clock signals can be output via a BNC connector to be monitored at a remote location. This capability proved to be very useful during the initial installation and commissioning. A second BNC output is driven by a current summing circuit to monitor the PMT pulses from selected channels.

In order that the contribution from the electronics not dominate the overall timing resolution of the system, a design goal of 25 ps for the intrinsic resolution of the electronics was set, one order of magnitude beyond what is needed for most other CDF-II electronics.

The stability of the entire electronics chain was initially studied by generating the common stop signal delayed with respect to a calibration pulse using a fixed length of cable. The resulting TDC distributions had typical RMS widths of 8.5 ps and their mean values were found to be stable at the level of 9 ps over the 40 hour duration of the study.

3 TOF Calibration

Without calibrating the response of each channel the timing resolution that can be achieved is of the order of a few nanoseconds. It is not possible to perform particle identification over any useful momentum range with a resolution this large.

The operation of a Time-of-Flight detector in the CDF-II environment is unique in that it is not possible to synchronize a timing signal with respect to the $p\bar{p}$ interaction time. This is a consequence of the ~ 30 cm length of the p and \bar{p} bunches in the Tevatron which yield interactions spread out in time by a few nanoseconds. Not only does this complicate particle identification but it also makes it difficult to determine the parameters needed to calibrate individual channels.

3.1 *On-line Calibration*

With such tight timing stability requirements, changes in the response of the electronics due to temperature variations, ground voltage shifts, or aging of the components are possible. The functionality for monitoring these effects is part of the electronics. Specifically, the time which corresponds to a particular value read out from the TAC is determined periodically in the "on-line" calibration runs taken during the time gap between consecutive Tevatron stores.

This calibration is performed using a digital delay generator DDG (Berkeley Nucleonics model B951) to initiate a differential ECL pulse that is fanned out to selected sets of channels. This signal is used to start the TAC, bypassing the discriminator. By stepping through a series of delays with respect to the common stop signal, the response of the TAC to known delays can be measured. Due to our demanding timing requirements we include a small non-linear correction to our TAC calibration, which is:

$$V_{TAC} = \beta(1 + \gamma e^{-t/\tau})t \quad (2)$$

where β , γ and τ are parameters determined from a fit to the set of generated delays. The deviation of the measurements from the fitted curve are gaussian distributed with a width of 5.1 ps. The parameterization adequately describes the response of all 432 channels in the system.

The TAC response has shown an excellent stability since the commissioning of the electronics. The readout time variations for a single DDG delay, remain within a 55 ps band over a six month period, even before applying the calibrations.

3.2 *Off-line Calibration*

Even for a ideal TOF detector where all its components are perfectly working, it is still necessary to correct for systematic effects intrinsic to the measurement method. The raw data registered from the $p\bar{p}$ collisions is analyzed off-line to characterize and correct such effects.

In this section, some of the most significant off-line corrections are summarized. This is a work still in progress, and further improvements are expected.

3.2.1 The timing model

The time t_i at which the discriminator of the channel i is fired, for a track hitting the scintillator at a position z along the length of the bar, is described by:

$$t_i = c_i + t_0 + tof + (L/2 \pm z)/s_j - S_i(Q_i) \quad (3)$$

where Q_i is the registered charge. The constant offset c_i includes, for example, propagation delays in the cables. The t_0 is the time with respect to the nominal bunch crossing. The tof is the particle's time of flight. The term $(L/2 \pm z/s_j)$ accounts for the light propagation time inside the bar j , being s_j the speed-of-light for this bar, (positive sign is for the west channels and the negative sign for the east channels). The last term describes the time-walk effect introduced by the use of leading edge pulse discriminators.

3.2.2 Time difference analysis

When a single track enters a bar of scintillator, the difference in the times read out on the east and west ends is essentially a linear function of z , the track's entrance point along the bar. A typical distribution of the time difference plotted as a function of z is shown in figure 3, the effective speed of light in the bar comes from the fitted slope. The distribution of the effective speed of light for all the bars is shown in 4.a.

The width of the residuals for this straight line fit are then a measure of the timing resolution of each PMT, added in quadrature. This resolution averaged over all bars is typically 250 ps or better, since this measures the resolution of two channels added in quadrature, it differs by approximately a factor of two from the resolution expected for a calculation of the mean time from which the time-of-flight is calculated. This indicates that our timing resolution is close to our design goals. However, as systematics effects can cancel in the calculation of the time difference measurement, but would not necessarily cancel in the calculation of time-of-flight, this estimate of the timing resolution only represents the intrinsic capabilities of the detector.

3.2.3 Attenuation length analysis

The response of the ADC was studied by selecting a sample of tracks passing through the front and back surfaces of the corresponding scintillator bar. The time difference, ΔT , was required to be within 1 ns of the time expected, based on the results of the analysis described in section 3.2.2 The ADC response on east and west ends were corrected for the path length of the track in the

scintillator and normalized to give the equivalent response from a track at normal incidence. An initial unbinned likelihood fit was performed in which the quantity $\log Q_{east}/Q_{west}$ was fit to a linear function of z . The slope parameter β , provided an initial estimate of the attenuation length in the bar, $\Lambda = 2/\beta$.

Although the ratio of the measured ADC responses has an exponential dependence on z , the ADC response of the individual east and west channels does not. Instead an additional factor with an exponential term proportional to z^2 is needed to describe the ADC response as a function of z which we hypothesize is due to reflection of light of the ends of the bars. These effects are shown for a typical PMT in Fig. 5, in which the distribution of the ADC response as a function of z is plotted along with the ADC response, corrected for the attenuation effects and fitted with a Landau distribution. The attenuation length measured for all the bars in the system ranges from 200 to 450 cm with a mean value of 330 cm.

3.2.4 Time slewing correction

The time slewing effect is due to the leading edge time pick-off method. Larger pulse height fire the discriminator at an earlier time than smaller pulse heights. The dependence between the pulse height on the measured time, has been studied using a sample where each track passes through two adjacent bars of scintillator. Depending on the path length in each bar, a range of ADC responses can be obtained in the two channels at the same ends of the bars. Because of the z -coordinate of the track's entrance point in each bar is similar, the time difference between the two channels would be nearly identical except for time slewing effects and transit time through the bar.

Equation 4 was found to describe adequately the slewing effect for channel i .

$$S_i(Q_i) = \alpha_i \frac{1}{\sqrt{Q_i}} \quad (4)$$

The time difference $T_a - T_b$ between two adjacent channels at the same ends of the bars, corrected by the time of propagation of the light from the entrance point to the bar ends, and by the different particle's time of flight between the two bar entrance points, would be identical except for the time slewing effect.

Figure 6 shows the dependence between the $T_a - T_b$ time difference with respect to the difference of the time slewing terms $S_a - S_b$. This dependence is essentially linear.

The slewing correction also introduced an linear dependence in the time difference $t_{east} - t_{west}$ versus the entrance point z , resulting in a biased effective speed of light determination. The time-walk-corrected speed of light is shown

in Fig. 4.b. After the correction is applied the width of the speed of light distribution is significantly reduced and the low values in the tail have disappeared.

4 Particle identification Performance

The analyses shown here are based in a logarithmic time slewing parameterization. Figure 7 show the mass distribution for tracks from a low momentum dimuon trigger. The mass was calculated using equation 1. The particle momentum and path-length to the TOF counter are from the central tracking drift chamber. Positively charged tracks are on the right, negative tracks are on the left. Three clear clouds corresponding to K , π and p can be seen.

Another measure of the performance of the entire TOF system can be obtained by analyzing the $\phi(1020) \rightarrow K^+K^-$ signal in a sample of events recorded with hadronic trigger[6]. Figure 8.a shows the reconstructed mass peak when $p_T < 1.5 GeV$ for both tracks. Figure 8.b shows the reduction in the background obtained by applying a 3σ cut on the quantity

$$w_K(t_K) = \frac{t_K - t_0}{\sqrt{\sigma_{t_K}^2 + \sigma_{t_0}^2}} \equiv \Delta t_K / \sigma_t \quad (5)$$

where t_K is the production time of a track, calculated using a kaon mass hypothesis, t_0 is the actual interaction time, and $\sqrt{\sigma_{t_K}^2 + \sigma_{t_0}^2}$ the error of its difference.

Although intended for B flavor tagging, the specialized analysis shown here is an example of a valuable TOF contribution in other areas. Other uses include cosmic rays rejection in high P_t dilepton physics and in exotics searches for extremely massive objects which are long-lived. A TOF based monopole trigger is being constructed

5 Summary

We have described the design of the CDF-II TOF system which was fully operational since August 2001. Since then, it has been working reliably without any significant problem.

Preliminary off-line and on-line calibrations have been summarized and initial performance have been shown. The time resolution design goal will be achieved

after a better understanding of the detector systematics based on the data analysis which is still in progress.

References

- [1] R. Blair et al., *The CDF-II Detector Technical Design Report*, FERMILAB-PUB-96/390-E
- [2] C. Paus et al., em Design and Performance Tests of the CDF Time- of-Flight System, *Nucl. Instrum. Meth.*, vol. A461, pp. 579-581, 2001.
- [3] C. Grozis et al., *The Time of Flight Detector at CDF*, *Nucl. Phys. Proc. Suppl.*, vol. 93, pp. 344-347, 2001.
- [4] C. Grozis et al., *A Time-of-Flight detector for CDF*, *Int.J.Mod.Phys. A16S1C:1119-1121*,2001.
- [5] T. Shaw, C. Nelson, and T. Wesson, *Design of the CDF Run 2 Calorimetry Readout Module*, *IEEE Trans. Nucl. Sci.*, vol. 47, pp. 1834-1838, 2000.
- [6] K. Anikeev et al., *B Physics at Tevatron : Run II and Beyond* FERMILAB Pub-01/197, hep-ph/0201071 December, 2001

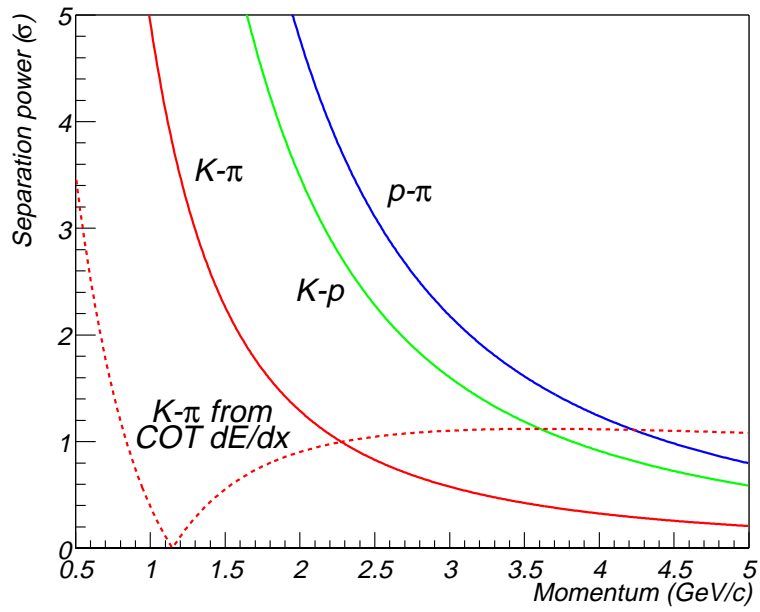


Fig. 1. Time difference as a function of momentum between K/π , p/K , and p/π for a path-length of 140 m. A resolution of 100 ps is assumed in the separation power axis. The dashed line shows the separation power of dE/dx measurement from the Central Outer Tracker

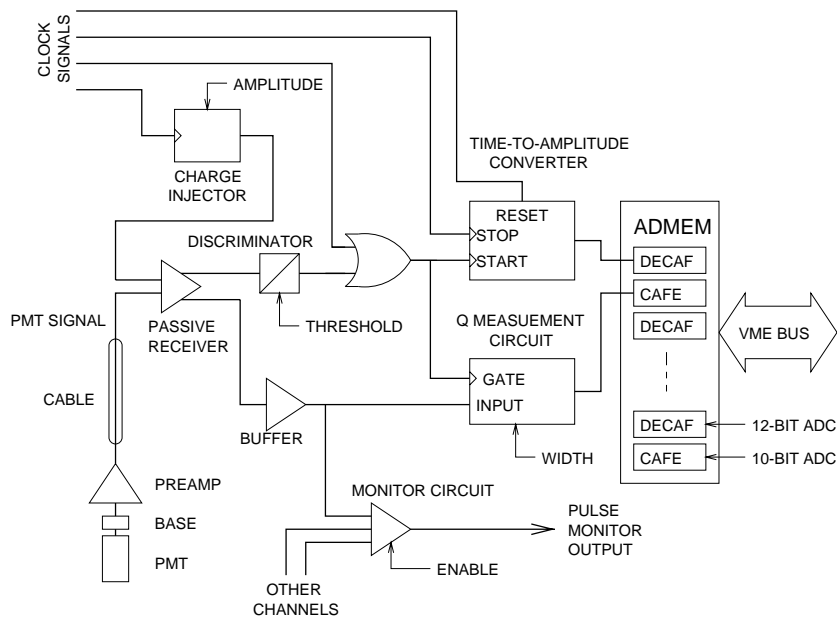


Fig. 2. A block diagram of the electronics processing chain for the signal from one PMT channel. Most of the signals are indicated by single lines for clarity but are actually differential signals.

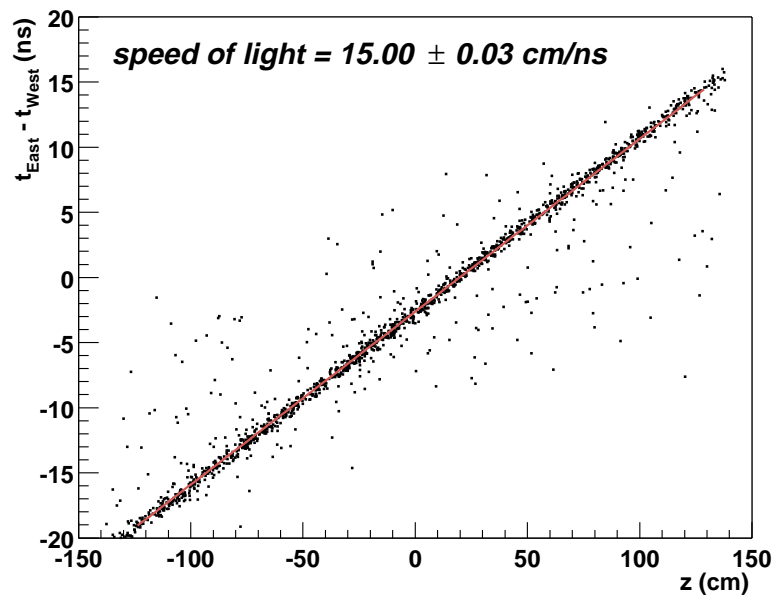


Fig. 3. Distribution of the time difference, $t_{east} - t_{west}$, plotted versus the entrance point, z , of a track. The scattered point away from the fitted line are due to multiple tracks hitting the bar.

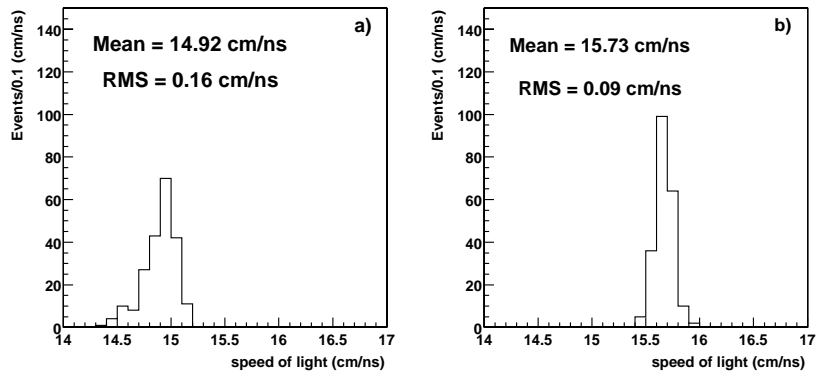


Fig. 4. (a) Effective speed of light distribution for all the bar before time slewing correction (b) Effective speed of light distribution for all the bar after time slewing correction

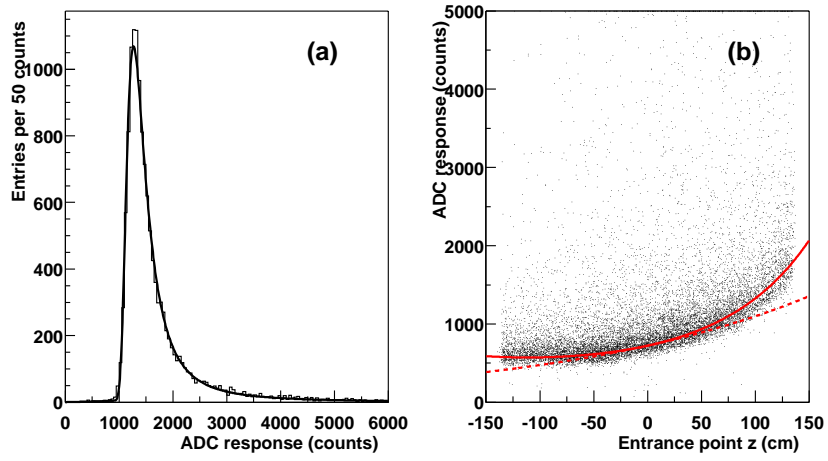


Fig. 5. (a) The ADC response, corrected for attenuation length effects, fit to landau function. (b) The distribution of ADC response as a function of z . The dotted curve is a pure exponential attenuation model, while the solid curve includes a z^2 term in the exponent

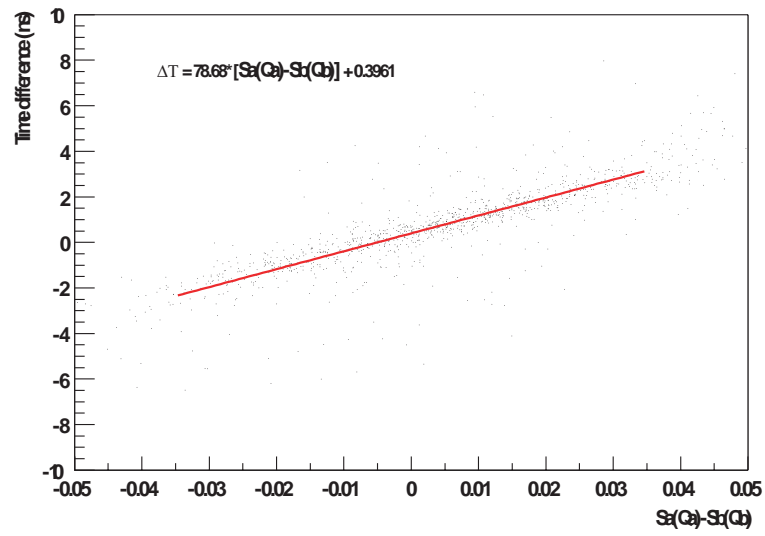


Fig. 6. Corrected time difference $T_a - T_b$ as a function of the difference of the time-slewing terms in two adjacent channels at the same ends of the bars.

CDF Time-of-Flight : Tevatron store 860 - 12/23/2001

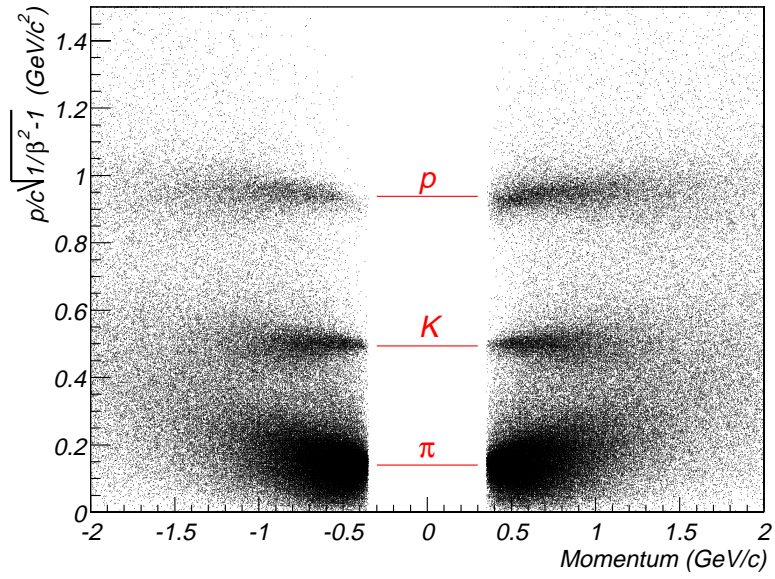


Fig. 7. Mass distribution from TOF measurement versus momentum, for positive and negative tracks. The three horizontal lines correspond to nominal p , K , and π masses.

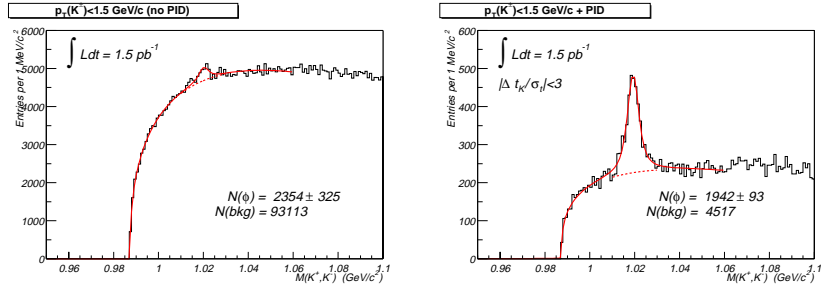


Fig. 8. (a) K^+K^- invariant mass distribution without particle ID (b) K^+K^- invariant mass distribution with TOF particle ID.